MANTLE SOURCE MINERALOGY INFERRED FROM INCOMPATIBLE ELEMENT RATIOS IN SHERGOTTITES. S. Yang[1], M. Humayun[1], K. Righter[2], A. J. Irving[3], R. H. Hewins[4,5] and B. Zanda[4,6]. [1]Florida State University, Tallahassee, FL 32310, USA (syang@magnet.fsu.edu); [2]NASA Johnson Space Center, Mail code XI2, Houston, TX 77058, USA; [3]Department of Earth and Space Sciences, University of Washington, Seattle, WA 98195, USA; [4]IMPMC, Sorbonne Université, MNHN-UPMC, 75005 Paris, France; [5]Rutgers University, Piscataway, NJ 08854, USA; [6]IMCCE, Observatoire de Paris - CNRS UMR 8028, 75014 Paris, France.

Introduction: The mineralogy of the martian mantle is a poorly known but vital compositional parameter. In the absence of samples of martian mantle peridotites, the mineralogy has been inferred from bulk composition constrained by a mix of cosmochemical and martian meteoritic constraints [1]. Such a mineralogy reflects the primordial mantle composition, but mantle source regions that differentiated from a magma ocean are not likely to have the same mineralogy as bulk silicate Mars [2-4]. An alternative approach is to infer source mineralogy of the martian mantle from the analysis of incompatible elements in shergottites. In a recent study [5], we showed that the general compatibility order of trace lithophile elements in martian mantle is similar to that of MORB mantle, with some exceptions. Compared to MORB mantle, in martian mantle: (1) highly incompatible elements (Th, Nb, Ta and U) are less incompatible relative to La; (2) K is significantly more compatible with respect to other elements; and (3) the HREEs are more compatible. In this study, we calculated effective partition coefficients of trace elements directly from martian igneous meteorites and used this data to infer the source mineralogy of the martian mantle.

Method: A logarithmic form of the batch melting equation (1) [6] was used to estimate partitioning behavior of incompatible trace elements:

$$\text{Log}\,[C_l^B\,] = \text{Log}\,\frac{1}{\frac{m}{[C_l^A\,]}+b} \qquad (1)$$

where [A] and [B] are concentrations of two elements (A and B) in mantle-derived magmas; and **b** and **m** are two terms that are related to source compositions (C_0) and partition coefficients (D) of elements A and B.

$$m=\left(\frac{C_0^A}{C_0^B}\right)\frac{1-D_B}{1-D_A} \quad ; \quad b=\frac{D_B-D_A}{C_0^B(1-D_A)} \qquad (2)$$

In this study, we applied this method to evaluate the partitioning behavior of trace elements in martian mantle. The Log [B] *vs.* Log [A] correlations of martian magmas were constrained using a shergottite dataset that is the most comprehensive to date, including 25 new LA-ICP-MS measurements [7-8]; 24 solution-ICP-MS [9] and all analyses from the Martian Meteorite Compendium [10]. Term **b** and **m** were solved by an iterative nonlinear regression method with MATLAB. Term **b** was used to find elemental pairs with the most similar compatibilities. The D_B was solved using the equation below:

$$D_B=\frac{b}{m}\times C_0^A + D_A \qquad (3)$$

Starting from a single reference element (i.e., La), a boot-strap method was used to calculate D of all available lithophile trace elements in shergottites (D_E). The values of C_0^{La} and D_{La} had to be arbitrarily chosen within reasonable value for Mars. The C_0^{La} used in our calculations were (1) 0.547 ppm of bulk silicate Mars (BSM) [1]; and (2) 0.153 ppm for the depleted martian mantle (DMAM). The DMAM value was calculated assuming DMAM is the residue of BSM [1] after the extraction of primitive martian crust [11]. The D_{La} (0.01) was arbitrarily assumed. The resulting D_E were normalized to D_{La}.

The effective bulk D_E for a trace element is related to the mineralogy of the source by weighting each mineral's D_i by its mass fraction (f_i):

$$\text{bulk } D_E = \sum_0^n D_i . f_i \qquad (4)$$

The bulk D_E/D_{La} of BSM for various published compositional models [1, 12-19] were calculated using experimentally determined *Di* compiled in this study (Fig. 1), and the modes (f_i) from the solidus mineralogy of each compositional model obtained by MELTS [20]. To compare the expected partitioning of modeled depleted martian mantle compositions proposed to form by crystallization of a magma ocean [21, 22], the bulk D_E/D_{La} of DMAM were calculated using mineralogy taken from [21, 22] and the partition coefficients used above.

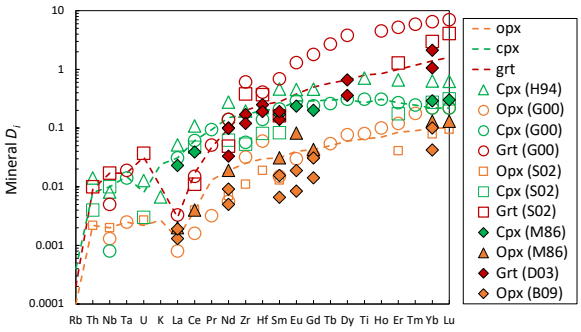

Fig. 1: The experimentally determined Ds of Cpx, Opx and Grt in martian compositions [23-25] and terrestrial compositions [26-28]. Dash lines represent D values used to calculate bulk Ds of shergottite mantle source.

To validate this approach, the same Log-Log procedure was applied to global MORB data [29] to calculate D_E/D_{La} in MORB mantle, which was then compared with D_E/D_{La} calculated using *Di* and mineral mode (f_i) of depleted MORB mantle (DMM) from [30].

Results: The calculated D_E/D_{La} using MORB data [29] agrees well with D_E/D_L calculated using D_i and

DMM f_i from [30] (not show), indicating correlations of Log [B] *vs.* Log [A] of basaltic lavas allow a meaningful assessment of source mineralogy.

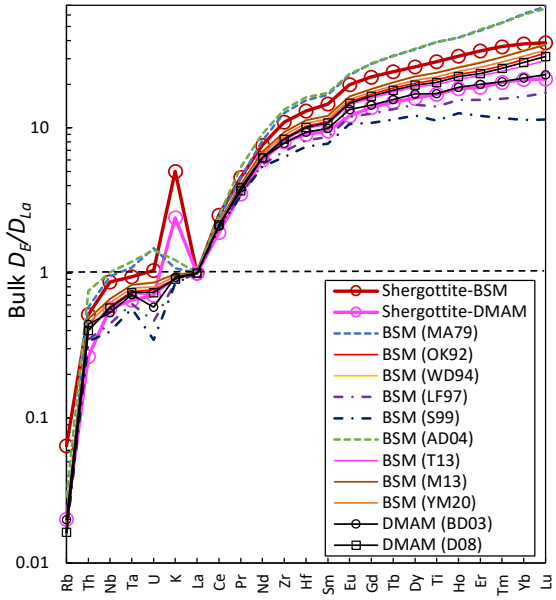

Fig. 2: The bulk D_i/D_{La} constrained by trace elemental concentrations in shergottites, along with that calculated using experimental D and source mineralogy.

The D_E/D_{La} pattern derived from shergottite data using C_0^{La} of BSM and DMAM are named as Shergottite-BSM and Shergottite-BMAM on Fig. 2. The D_E/D_{La} pattern obtained using experimentally determined D_i (Fig. 1) and solidus mineral modes (f_i) of modeled martian compositions [1, 12-19] obtained by MELTS [20] are named using author's initials with publication years on Fig. 2. The D_E/D_{La} pattern obtained using the same D_i and mineralogy of DMAM [21, 22] are named using the same format on Fig. 2.

Discussion: In a companion study [20], we used model compositions of bulk Mars [1, 12-19] to model the solidus mineralogy of martian mantle. The slopes of D_E/D_{La} of each model composition of Mars [1, 12-19] are determined by the solidus mineralogy, particularly the garnet abundances [20]. Our results show that compositions with low Al_2O_3/SiO_2 ratios (e.g., LF97 and S99) [15, 16] yield mineralogy that has little or no garnet, whereas compositions with high Al_2O_3/SiO_2 ratio (e.g., MA79) [12] yield mineralogy that have the highest garnet modal abundances (~ 20 wt.%). This explains the offsets between MA79 curve and the curves of LF99 and S99 observed in Fig. 2. As shown in Fig. 1, relative to D_{La}, elemental D_i of some highly incompatible elements (e.g., Nb, Ta, U) and of HREEs are more compatible in garnet than in pyroxene. Thus, the pattern of bulk D_E/D_{La} of martian mantle (Fig. 2) is sensitive to the garnet mode in the source region.

Here we show the comparison between bulk D_E/D_{La} directly constrained using shergottite data and that calculated from bulk compositional models yields insights into the mantle mineralogy of shergottite source region: (1) compositional models that have low garnet abundances [15, 16] yielded curves (LF97 and S99) cannot match the shergottite-constrained curves for any assumption of C_0^{La} ; (2) a DMAM with 3 % garnet (BD03) [21] matches the shergottite-constrained curve (assuming C_0^{La} of DMAM), while a DMAM with 10 % garnet [22] yielded curve (D08) with higher D_E/D_{La} of HREEs; (3) compositional models [1, 13, 14, 17, 19] that have ~10 % garnet yielded curves (OK92, WD94, T13, M13, YM20) that are close to the shergottite-constrained curves assuming C_0^{La} of BSM [1]; and (4) the compositional model that has the highest garnet abundance (~ 25 %) [12] yielded a curve (MA79) that has too high D_E/D_{La} of U and HREEs to match shergottite-derived curves. But none of modeled curves can account for the significantly elevated D_K in shergottites (Fig. 2). The existence of a minor high-pressure phase that makes K highly compatible in the shergottite source is implied. In this study, we showed that trace element compositions of shergottites are indicators of source mineralogy and that the shergottite source is consistent with primitive martian mantle.

References: [1] Yoshizaki T., & McDonough W. F. (2020) *GCA 273,* 137-162. [2] Debaille V. et al. (2007) *Nature 450.7169,* 525-528. [3] Elkins-Tanton L. T. (2008) *EPSL 271,* 181-1. [4] Elkins-Tanton L. T. et al. (2003) *MaPS 38,* 1753-1771. [5] Yang S. et al. (2021) LPSC LII abstract #1646. [6] Sims K. W., & DePaolo D. J. (1997). *GCA 61,* 765-784. [7] Yang S. et al. (2015) *MaPS 50,* 694-714. [8] Yang S. et al. (2020) LPSC LI abstract #1300. [9] Day J.M. D. et al. (2018) *Nat. Commun. 9,* 1-8. [10] Righter K. (2017) Martian Meteorites Compendium. [11] Humayun M. et al. (2013) *Nature 503.7477,* 513-516. [12] Morgan J. W., & Anders E. (1979). *GCA 43,* 1601-1610. [13] Ohtani E., & Kamaya N. (1992). *GRL 19,* 2239-2242. [14] Wänke H., & Dreibus G. (1994) *Series A: Phys. Eng. Sci.* 349.1690, 285-293. [15] Lodders K., & Fegley B. (1997) *Icarus 126,* 373-394. [16] Sanloup C. et al. (1999) *Phys. Earth Planet. Inter. 112,* 43-54. [17] Taylor G. J. (2013) *Geochemistry 73,* 401-420. [18] Agee C. B., & Draper D. S. (2004) *EPSL 224,* 415-429. [19] Matsukage K. N. et al. (2013) *J. Mineral. Petrol. Sci.* 120820. [20] Yang S. et al. (2022a) LPSC LIII abstract (submitted). [21] Borg L. & Draper D. S. (2003) *MaPS 38,* 1713-1731. [22] Debaille V. et al. (2008) *EPSL* 269, 186-199. [23] McKay G. et al. (1986) *GCA 50,* 927-937. [24] Draper D. S. et al. (2003) *Phys. Earth Planet. Inter. 139,* 149-169. [25] Blinova A. and Herd C. (2009) *GCA 73,* 3471-3492. [26] Hauri E. H. et al. (1994) *Chem. Geol. 117,* 149-166. [27] Green T. H. et al. (2000) *Lithos 53,* 165-187. [28] Salters V.J. et al. (2002) *G^3 3,* 1-23. [29] Yang S.et al. (2020) *Sci. Adv. 6,* eaba2923. [30] Salters V. J., & Stracke A. (2004) *G^3 5,* (5)